HHS Public Access

Author manuscript

J Fluor Chem. Author manuscript; available in PMC 2018 June 01.

Published in final edited form as:

J Fluor Chem. 2017 June ; 198: 10–23. doi:10.1016/j.jfluchem.2016.12.016.

Strategic Incorporation of Fluorine into Taxoid Anticancer Agents for Medicinal Chemistry and Chemical Biology Studies

Iwao Ojima[1,2,*]

[1]Department of Chemistry, State University of New York at Stony Brook, Stony Brook, NY, 11794-3400, U. S. A

[2]Institute of Chemical Biology & Drug Discovery, State University of New York at Stony Brook, Stony Brook, NY, 11794-3400, U. S. A

Abstract

This account exemplifies our recent progress on the strategic incorporation of fluorine and organofluorine groups to taxoid anticancer agents and their tumor-targeted drug delivery systems (TTDDSs) for medicinal chemistry and chemical biology studies. Novel 3′-difluorovinyltaxoids were strategically designed to block the metabolism by cytochrome P-450, synthesized, and evaluated for their cytotoxicity against drug-sensitive and multidrug-resistant (MDR) human cancer cell lines. 3′-Difluorovinyltaxoids exhibited impressive activities against these cancer cell lines. More significantly, a representative 3′-difluorovinyltaxoid exhibited 230-33,000 times higher potency than conventional anticancer drugs against cancer stem cell-enriched HCT-116 cell line. Studies on the mechanism of action (MOA) of these fluorotaxoids were performed by tubulin polymerization assay, morphology analysis by electron microscopy (EM) and protein binding assays.

Novel ^{19}F NMR probes, BLT-F_2 and BLT-S-F_6, were designed by strategically incorporating fluorine, CF_3 and CF_3O groups into tumor-targeting drug conjugates. These ^{19}F-probes were designed and synthesized to investigate the mechanism of linker cleavage and factors that influence their plasma and metabolic stability by real-time ^{19}F NMR analysis. Time-resolved ^{19}F NMR study on probe BLT-F_2 revealed a stepwise mechanism for the release of a fluorotaxoid, which might not be detected by other analytical methods. Probe BLT-S-F_6 were very useful to study the stability and reactivity of the drug delivery system in human blood plasma by ^{19}F NMR. The clean analysis of the linker stability and reactivity of drug conjugates in blood plasma by HPLC and ^{1}H NMR is very challenging, but the use of ^{19}F NMR and suitable ^{19}F probes can provide a practical solution to this problem.

Graphical Abstract

This account presents our recent progress on the strategic incorporation of fluorine and organofluorine groups to new-generation taxoid anticancer agents and their tumor-targeted drug

*Corresponding author. Tel: +1-631-632-1339; Fax: +1-631-632-7942. iwao.ojima@stonybrook.edu.

delivery systems (TTDDSs), as well as an application of ^{19}F NMR for the assessment of metabolic stability of TTDDSs by exploiting the unique nature of fluorine.

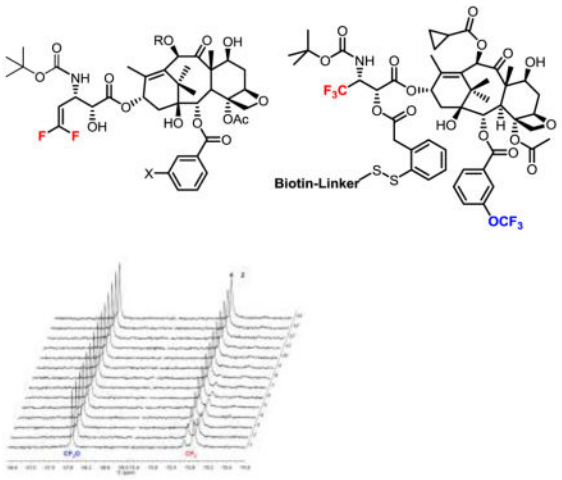

Keywords

Taxoid; Anticancer agent; Fluorotaxoid; Structure-activity relationship; ^{19}F NMR; Plasma and metabolic stability; Tumor-Targeted Drug Delivery System

1. Introduction

It is evident that fluorine plays a significant role in medicinal chemistry, chemical biology and drug discovery, which is supported by the fact that a large number of fluorine-containing compounds have been approved by the FDA for medical and agricultural use [1–5]. In fact, in the current drug design and discovery, fluorine is ranked second after nitrogen as “favorite heteroatom” [6]. The replacement of a C-H or C-O bond with a C-F bond in medicinally active compounds has been often found to introduce or improve desirable pharmacological properties such as higher metabolic stability, increased binding to target molecules, and enhanced membrane permeability [7, 8]. The special properties that make fluorine and organofluorine groups very attractive in medicinal chemistry and chemical biology include small atomic radius, high electronegativity, nuclear spin of ½, and low polarizability of the C–F bond. Thus, in the current drug discovery and development, it is common to explore fluorine-containing analogs of lead compounds for optimization.

This account presents our recent progress on the strategic incorporation of fluorine and organofluorine groups to new-generation taxoid anticancer agents and their tumor-targeted drug delivery systems (TTDDSs), as well as an application of ^{19}F NMR for the assessment of metabolic stability of TTDDSs by exploiting the unique nature of fluorine.

Despite huge investment and advancements in clinical and basic research over the decades, cancer remains as one of the most challenging diseases for effective treatments and cure. One of the critical issues in the conventional chemotherapy is the undesirable side effects, which affect patient’s quality of life. The solutions to this issue can be found in “targeted

cancer therapy". Traditional chemotherapy relies on the assumption that rapidly proliferating cancer cells are more sensitive to cytotoxic agents than normal cells. However, unfortunately, these cytotoxic agents have little or no specificity, causing systemic toxicity, which leads to undesirable side effects. Therefore, the development of tumor-specific drugs or drug delivery systems for anticancer agents, differentiating the normal and cancer cells or tissues, is an urgent need to significantly mitigate adverse effects associated with cancer chemotherapy. Rapidly proliferating cancer cells overexpress cancer-specific receptors to promote the uptake of nutrients and vitamins. These receptors can be used as targets for cancer-specific delivery of cytotoxic agents through receptor-mediated endocytosis (RME). Moreover, the unique physiology specific to tumor and cancer cells can be exploited to selectively accumulate and release a cytotoxic agent inside cancer cells. Accordingly, a variety of tumor-targeted drug delivery systems have been developed over a few decades [9–14].

A tumor-targeted drug delivery system (TMDDS) is composed of a tumor-targeting module (TTM) and a cytotoxic drug connected through a suitable linker and/or a vehicle material. These drug conjugates should be stable in blood circulation to minimize systemic toxicity, but efficiently internalized into the target cancer cells through RME. Then, the cytotoxic agent should be efficiently released from the drug conjugate without loss of potency [9, 14–17]. Since the specificity of TTDDS is achieved by cancer-specific TTM, highly potent cytotoxic agents can be used even when those agents do not have wide therapeutic window.

Besides the quality of life issue in conventional chemotherapy, there is another serious problem that needs to be addressed. It is the control and eradication of "cancer stem cells". In the last decade, the ineffectiveness of conventional chemotherapeutic drugs has been attributed to the existence of relatively rare, highly drug-resistant, quiescent or slowly proliferating tumor-initiating cells, termed "cancer stem cells (CSCs)" [18]. Through successful isolation and characterization of CSCs from all major types of human tumors, it has become evident that CSCs are exclusively endowed with tumor-initiating capacity in the majority, if not all, cancer types. More importantly, there is every indication that CSCs are responsible for tumor sustaining, resistance to treatment, metastasis and recurrence [18]. CSCs induce to a variety of proliferating, but progressively differentiating tumor cells, contributing to the cellular heterogeneity of human cancers. Therefore, it appears that CSCs represent the most crucial target in the development of a next generation anticancer drugs [19, 20].

Paclitaxel (Taxol®) and docetaxel (a "taxoid") are two of the most extensively used chemotherapeutic agents in clinic [21]. In many of their clinical indications, paclitaxel or docetaxel is combined with one or more additional anticancer agents. Recently, another taxoid, cabazitaxel, was approved by the FDA for hormone-refractory prostate cancer in combination with prednisone [22]. In addition to these FDA-approved drugs, a number of novel taxoids are in various stages of clinical and preclinical development [23, 24].

Although these drugs have made significant impact on cancer chemotherapy, their utility is limited due to their susceptibility to multidrug resistance (MDR) and lack of tumor specificity. For example, these drugs show little to no efficacy against melanoma, colon,

pancreatic and renal cancers [25]. Human colon carcinoma overexpresses ATP-binding cassette transporter proteins, such as the P-glyocoprotein (Pgp), which leads to intrinsic MDR [26]. The Pgp binds hydrophobic molecules and acts as an efflux pump, reducing their intracellular concentration [27]. Based on extensive structural-activity relationship (SAR) studies, we have developed a series of highly potent new-generation taxoids, including "fluorotaxoids" [28–33]. Many of these taxoids exhibit improved activity against drug-sensitive cancer cell lines, as well as two 2–3 orders of magnitude higher potency against drug-resistant cancer cell lines [28–30].

Fluorotaxoids certainly serve as potent anticancer agents for TTDDS. Fluorine can also be strategically incorporated to provide novel biochemical tools that are useful for the development of TTDDSs [15, 34]. For instance, by taking advantage of the fact that the fluorine nucleus is virtually non-existent in biological systems, ^{19}F NMR can provide techniques to directly observe time-dependent processes in complex biological systems [35].

2. Design and synthesis of novel difluorovinyltaxoids with high potency against MDR cancer cell lines and cancer stem cells

Our extensive SAR studies of taxoid anticancer agents have led to the discovery and development of new-generation taxoids bearing non-aromatic substituents (isobutenyl or isobutyl) at the C3′ position and various acyl groups at the C10 position [30, 36], as well as *meta*-substituted benzoyl groups at the C2 position [30, 37]. These taxoids exhibited 2–3 orders of magnitude higher potency than paclitaxel and docetaxel against MDR cancer cell lines [30, 36, 37]. We have also designed and synthesized novel 3′-trifluoromethyl- and 3′-difluoromethyltaxoids with C10 as well as C10/C2 modifications in a similar manner [31, 38, 39]. The evaluation of their potencies showed that trifluoromethyl and difluoromethyl groups were viable modifiers of the C3′ position and a number of highly potent fluorotaxoids were identified. Nevertheless, the isobutenyl group was found to be the best substituent at C3′ for cytotoxicity. However, our study on the metabolic stability of 3′-isobutyl- and 3′-isobutenyl-taxoids revealed that there was a marked difference in metabolism between the new-generation taxoids and that of docetaxel and paclitaxel [40]. The metabolism study showed that CYP 3A4 in the cytochrome P450 family in humans metabolized these taxoids such as SB-T-1214 and SB-T-1216, through hydroxylation primarily at the two allylic methyl groups of the 3′-isobutenyl group (Fig. 1).

2.1. Design and synthesis of 3′-difluorovinyltaxoids

As mentioned above, the primary metabolism of new-generation taxoids that bear a 3′-isobutenyl group was found to be the hydroxylation of the allylic methyl groups by CYP3A4 [40]. Thus, in order to prevent this allylic hydroxylation, we planned to introduce a difluorovinyl group in place of the 3′-isobutenyl group by mimicking it [32].

2.1.1. Molecular modeling of 3′-difluorovinyltaxoids in β-tubulin—To probe the bioactive conformations of the designed 3′-difluorovinyltaxoids, SB-T-12853 was selected as representative, and docked to the paclitaxel binding site in the β-tubulin subunit using the "REDOR-Taxol" coordinates [41, 42]. The binding energy of the system was minimized

(InsightII 2000, CVFF) wherein the protein backbone was fixed, but the side chains were allowed to find their lowest energy conformations. The "parent" taxoid, SB-T-1213, was also docked into β-tubulin following the same protocol for comparison. The resulting computer-generated binding structures of these taxoids and their overlay are shown in Fig. 2.

As Fig. 2 shows, these two taxoids form a very stable H-bond with His227, consistent with the REDOR-Taxol structure. The overlay (Fig. 2b) of SB-T-12853 and SB-T-1213 structures shows virtually complete overlap in their baccatin moieties, but a small yet appreciable difference in the side chain positions. The result indicates that difluorovinyl group would nicely mimics isobutenyl group in spite of a difference in size and electronic nature between two groups. The size of the difluorovinyl group is between vinyl and isobutenyl groups and two fluorine atoms would mimic electronically two hydroxyl groups rather than two methyl groups. In any case, the computational analysis provided a strong rationale to synthesize the designed novel difluorovinyltaxoids and examine their biological activities.

2.1.2. Synthesis of novel 3′-difluorovinyltaxoids—A series of novel 3′-difluorovinyltaxoids **1** were synthesized through the Ojima-Holton coupling of enantiopure (3*R*,4*R*)-4-difluorovinyl-β-lactam **3** with various baccatins **2** with modifications at 10 and/or 2 positions in 49–96% yields (Scheme 1) [32]. 10-Modified baccatins **2** (X = H) [36] and 2,10-modified baccatins **2** (X = MeO, N_3, F, Cl) [30] were prepared using the methods reported previously by our laboratory. Enantiopure (3*R*,4*R*)-4-difluorovinyl-β-lactam **3** was prepared from enantiopure (3*R*,4*S*)-4-isobutenyl-β-lactam **3**, which was obtained by the method reported previously from our laboratory, through ozonolysis, difluoromethylene-Wittig-type reaction and CAN reaction in good overall yield (Scheme 2) [32].

2.2. Cytotoxicity of 3′-difluorovinyltaxoids

3′-Difluorovinyltaxoids exhibit impressive potencies against human breast, ovarian, colon and pancreactic cancer cell lines (Table 1) [32]. It has also been shown that these fluorotaxoids initiate apoptosis primarily *via* the activation of caspases 2, 8 and 9 [43]. As Table 1 shows, 3′-difluorovinyltaxoids exhibit one order of magnitude and up to three orders of magnitude higher potency as compared to that of paclitaxel against MCF-7 (drug-sensitive) and NCI/ADR (drug-resistant) cancer cell lines, respectively.

2.3. Remarkable activities of 3′-difluorovinyltaxoids against cancer stem cells (CSCs)

New-generation taxoid, SB-T-1214, demonstrated remarkable efficacy in drug-resistant cancers both *in vitro* and *in vivo* [30]. SB-T-1214 was also found to exhibit excellent activity against spheroids derived from highly drug-resistant cancer stem cells (CSCs) [19]. A fluorotaxoid, SB-T-12854, was also found to be highly potent against CSC-enriched HCT-116 human colon cancer cells. A comparison of potencies between conventional anticancer drugs and new-generation taxoids is summarized in Table 2 [44]. As Table 2 shows, it is impressive that SB-T-12854 exhibits 230-33,000 times higher potency than conventional anticancer drugs against CSC-enriched HCT-116 cell lines. As described above, CSCs are believed to be responsible for tumor metastasis and reoccurrence [45], this finding is quite significant. It has been indicated that the new-generation taxoids, exhibiting high potency against CSCs, suppress the expression of "stemness genes", promoting

differentiation of the treated CSCs [19], which may provide a new mechanism of action (MOA) for taxoid anticancer agents whose major MOA is the blocking of the cell mitosis at the G2/M stage, leading to the activation of caspases and then apoptosis [43, 46–48].

The ability of new-generation fluorotaxoids exemplified by SB-T-12854 to critically damage CSC populations clearly indicates the merit in the use of these fluorotaxoids for TTDDSs, as well as drug combinations and nanoformulations.

2.3. Tubulin polymerization and microtubule stabilization by 3′-difluorovinyltaxoids

Three difluorovinyltaxoids, SB-T-12851, SB-T-12853 and SB-T-12854, were examined for their potencies in tubulin polymerization and microtubule stabilization in comparison to paclitaxel. As Fig. 3 show, these difluorovinyl taxoids induced GTP-independent tubulin polymerization much faster than paclitaxel, and the tubulin polymerization caused by difluorovinyltaxoids reaches a plateau quickly and does not change with time. This may suggest that the microtubules formed by the action of these difluorovinyltaxoids have different properties from those formed by paclitaxel. As is well known for paclitaxel, the resulting microtubules were stable to Ca^{2+}-induced depolymerization.

Since the assembly induction was monitored by turbidity and this technique would be affected by the morphology of the polymers, it is rather difficult to know if the effect of these fluorotaxoids on the microtubule assembly was only to increase the rate of the assembly or if it also increased the mass of microtubules formed. Thus, the critical concentration of tubulin required for assembly induction in the presence of SB-T-12854 was determined and compared with those for paclitaxel and SB-T-1214 using centrifugation and quantification of the microtubules formed [47] (Table 3). Apparently, SB-T-12854 induced tubulin assembly with much higher potency than paclitaxel and docetaxel, and even three times higher potency than SB-T-1214. Thus, it is indicative that not only the rate of assembly was faster but also a larger number of microtubules was formed.

In order to correlate the observed cytotoxic effect of paclitaxel, SB-T-1214 and SB-T-12854 with their affinity to microtubules, the binding constants of these compounds were determined using the fluorescent ligand displacement method [47]. As Table 4 shows, the binding of SB-T-12854 is ca. 10 times stronger than paclitaxel and slightly better than SB-T-1214. Then, the thermodynamic parameters of the interaction, i.e., free energy of the binding (ΔG) and the enthalpy (ΔH) and entropy (ΔS) contributions to ΔG were calculated based on the binding constants [47]. As Table 5 indicates, the binding of SB-T-1214 and SB-T-12854 are much less exothermic with a large decrease in the enthalpy of binding, but this decrease in the enthalpy of binding is compensated by a substantial increase in the entropy of binding, which suggests significant differences in the binding mechanism.

2.4. EM analysis of microtubules treated with selected difluorovinyltaxoids

Microtubules formed by the action of difluorovinyltaxoids were analyzed by electron microscopy (EM) to examine their morphology and structure [32]. Microtubules formed using GTP or paclitaxel were used as standards for comparison purposes. The electron micrographs of microtubules formed in the presence of SB-T-12851, SB-T-12852, SB-T-12854, paclitaxel and GTP are shown in Fig. 4. Microtubules formed in the presence of

GTP and paclitaxel are long and thick (Fig. 4a and 4b), while in contrast those formed by the action of difluorovinyltaxoids (Fig. 4c, 4d and 4e) are much thinner and shorter in length, which indicates substantial difference in their properties as compared to those formed by the action of paclitaxel or GTP. It is strongly suggested that the formation of numerous thinner and shorter microtubules is related to the rapid polymerization of tubulin with these difluorovinyltaxoids (see Fig. 3). Some morphological similarity is observed between those microtubules arising from the treatment of tubuline with difluorovinyltaxoids and those with new-generation taxoids such as SB-T-1213 and SB-T-1214 [30]. However, the formation of a large number of thinner, shorter and straight microtubules appears to be unique to difluorovinyltaxoids.

2.5. Metabolism of Difluorovinyltaxoids

The metabolic stability of 3′-difluorovinyltaxoids against P-450 family enzymes was examined and it was found that almost no appreciable metabolites were formed [49]. The results indicate that not only the metabolism at C3′ is effectively blocked, but also oxidative metabolism is suppressed on other parts of the taxoid molecule, including the C3′N-*t*-Boc and C6 methylene moieties [49], which are known to be the major metabolism sites for docetaxel and paclitaxel [50–52]. Consequently, our strategic incorporation of a difluorovinyl group in place of an isobutenyl group at C3′ has been proven to be successful in blocking the major metabolism of the isobutenyl moiety in the new-generation taxoids (see Fig. 1).

3. Fluorine-Labeled Taxoids as ^{19}F NMR Probes for the Metabolic Stability Assessment of Tumor-Targeted Drug Delivery Systems

As mentioned in the Introduction, extensive efforts have been made on the development of tumor-targeted drug delivery systems (TTDDSs), exploiting the unique and intrinsic physiological and biochemical properties of tumors and cancer cells to selectively deliver cytotoxic drugs to cancer cells [14, 16]. A TTDDS is made of a tumor-targeting moiety (TTM) and a cytotoxic drug connected through a “smart” linker system. A smart linker system must be stable in blood circulation, but should be readily cleaved to release the free cytotoxic drug upon internalization into cancer cells or accumulation in the tumor microenvironment. Because of the critical importance of linker dynamics for TTDD efficacy, various smart linker systems have been developed in the last two decades, in particular for antibody–drug conjugates (ADCs) [9, 12, 53–57] and small-molecule drug conjugates (SMDCs) [9, 17, 58–60]. In this regard, we have developed novel self-immolative disulfide linkers that can release unmodified cytotoxic drugs via glutathione-triggered linker cleavage, involving thiolactonization [15–17, 61–63].

It is possible for ^{19}F NMR spectroscopy to directly observe fluorinated compounds and their metabolites in biological systems without background signal from the tissue or medium because of the absence of fluorine in living systems [1]. Moreover, the natural abundance of ^{19}F is 100% and ^{19}F is highly sensitive to NMR detection (83% of ^{1}H), which makes it possible to observe a strong NMR signal with negligible background noise [64]. As one of the notable advances in the applications of ^{19}F NMR spectroscopy to chemical biology, the

"three fluorine atoms biochemical screening (3-FABS)" has emerged in the last decade as a useful biochemical tool with heightened signal sensitivity by labeling a substrate with a CF_3 moiety for the analysis of enzymatic processes [65–67].

We have been designing and applying "fluorine-probes" for structural analysis of paclitaxel and taxoids in the absence and presence of microtubules by ^{19}F NMR in solution and solid state, as well as in combination with computational analysis [41, 42, 68–71] We also applied time-resolved ^{19}F NMR spectroscopy to show a proof of concept for the mechanism-based drug release through thiol-triggered cleavage of a self-immolative disulfide linker and subsequent thiolactionization, using a model system [15] (Fig. 5).

Fig. 6 exemplifies a series of taxoid-based TTDDSs using self-immolative disulfide linkers, which have been successfully developed in our laboratory [16, 17, 60, 61]. These TTDDSs, targeting vitamin B receptors, are efficiently internalized via RME that transfer the drug conjugates through endosomal and lysosomal compartments. It has been shown that the concentration of endogenous thiols, represented by glutathione (GSH), in these compartments is >1,000 times higher (2–8 mM) than that in the blood stream (1–2 μM) [72, 73]. GSH and other thiols trigger the drug release cascade of the self-immolative linker system via the cleavage of disulfide linkage and thiolactonization (see Fig. 5) [16]. The internalization of TTDDSs via RME and designed drug release inside cancer cells were clearly visualized and validated by confocal fluorescence microscopy (CFM) and flow cytometry analyses, using fluorescence-labeled TTDDSs [16, 17, 60, 61].

3.1. Design and synthesis of ^{19}F NMR probes, BLT-F_2 and BLT-S-F_6

We designed and synthesized two novel ^{19}F NMR probes, BLT-F_2 and BLT-S-F_6 in order to investigate the factors that influence the rate of disulfide cleavage and drug release in biologically relevant media such as human blood plasma [74]. This type of assessment by conventional HPLC or ^{1}H NMR analysis would be challenging, due to complex background peaks/signals. BLT-F_2 and BLT-S-F_6 are TTDDSs, consisting of fluorotaxoids, SB-T-12145 and SB-T-12822-5, respectively, as cytotoxic agents, a self-immolative disulfide linker unit, and biotin as the tumor-targeting module (Fig. 7). Fluorine, CF_3 and CF_3O groups were strategically incorporated into each conjugate to monitor the dynamics of disulfide linker cleavage and drug release by ^{19}F NMR.

3.1.1. Synthesis of BLT-F_2—For the construction of BLT-F_2, fluorotaxoid SB-T-12145 was synthesized first as a close mimic of a highly efficacious next-generation taxoid, SB-T-1214 [19, 20, 30, 36], through the Ojima-Holton coupling of fluorobaccatin **6** with β-lactam **7** (Scheme 3) [74]. The linker construct **12**, incorporating another fluorine at the 4 position of the disulfanylphenylacetate moiety, i.e., *para* to the disulfide moiety was synthesized from 5-fluorobenzothiophene (**8**) via 5-fluoro-2-surfhydrylphenylacetic acid (**10**) (Scheme 4) [74]. Finally, BLT-F_2 was assembled by coupling SB-T-12145 with linker construct **12**, followed by the activation of the resulting carboxylic acid **13** as *N*-hydroxysuccinimide ester, and subsequent amide coupling of the activated ester with biotinhydrazide (Scheme 5) [74].

3.1.2. Synthesis of BLT-S-F_6—BLT-S-F_6 was designed as a more sensitive ^{19}F NMR probe than BLT-F_2 by introducing CF_3 and CF_3O groups as reporter signals [74]. Also, in order to increase the aqueous solubility, a triethylene glycol moiety, "PEG_3", was introduced to the linker unit. We hypothesized that there should be a significant difference in chemical shift between the CF_3 group in the free taxoid, SB-T-12822-5, and the taxoid moiety in BLT-S-F_6 since the CF_3 group at C3′ of the taxoid moiety is located adjacent to the site of linker attachment, i.e., the hydroxyl group at C2′. On the other hand, we thought that the CF_3O group attached to the meta position of the benzoate moiety at C2 would serve as excellent internal standard.

SB-T-12822-5 was synthesized through the Ojima-Holton coupling of CF_3O-baccatin 14 with CF3-β-lactam **15** [31] (Scheme 6) [74]. BLT-S-F_6 was assembled by coupling SB-T-12822-5 with linker construct **16** [17], followed by amide coupling of construct **17** with biotinyl-NH-PEG_3-$(CH_2)_2NH_2$ (Scheme 7) [74].

3.2. ^{19}F NMR analysis of the linker cleavage and drug release using BLT-F_2

Fig. 8 illustrates the time-resolved ^{19}F NMR spectra of disulfide linker cleavage in BLT-F_2 in aqueous DMSO solution (30% DMSO, 70% D_2O) at 25 °C, starting from *1 hour after* the addition of GSH (6 eq, 15 mM) at 25 °C with 15 minute intervals [74]. The reference signal of the fluorine atom in the C2-benzoate group of SB-T-12145, as well as in the taxoid moiety of BLT-F_2 was clearly identified at −112.5 ppm, indicating no appreciable chemical shift change during the process under the conditions employed. Although it is clear that most of BLT-F_2 (at −114.1 ppm) was consumed after incubation with GSH for 1 hour, the disappearance of BLT-F_2 did not directly correspond to the formation of thiolactone **9** (at −116.3 ppm). This observation is in sharp contrast to that in the model system shown in Fig. 5. The ^{19}F NMR analysis revealed a substantial formation of 2′-fluoro(sulfhydryl)phenylacetyltaxoid **18** (at −119.2 ppm) at the beginning of the monitoring as a key transient species of this process. The formation of thiolate at *para* to the position of fluorine in the phenylacetate moiety is rationalized by the observed 5 ppm upfield shift in this fluorine signal. Then, the thiolactonization of **18** took place to form free taxoid SB-T-12145, which is apparent from the observed decrease in the **18** signal and the increase in the free taxoid signal over the time course.

This study disclosed that the cleavage of the disulfide linker proceeded in two steps, forming a mechanistically anticipated thiolate **18** as detectable transient species, prior to thiolactonization [74]. The introduction of a fluorine *para* to a disulfide linkage should have a profound effect on the rate of linker cleavage as well as thiolactonization. The *para*-fluorine can stabilize the thiolate being formed, which may contribute to faster disulfide cleavage in the thiol-disulfide exchange process, and also slower thiolactonization by reducing the nucleophilicity of the thiolate species. The fact that the 2-step process was not observed in the model system (see Fig. 5) may indicate that the steric and/or conformational microenvironment in BLT-F_2 are substantially different from those of the model system. Consequently, it is worthy of note that BLT-F_2 provided unique and very useful information for the mechanism of "self-immolation", which would not have been possible by other means.

Initial attempt to use BLT-F_2 as a ^{19}F NMR probe in cell culture media or blood plasma (10% DMSO, 20% D_2O, 70% plasma/media) was unsuccessful due to the poor solubility and low signal intensity of the probe [74]. Nevertheless, we found that the use of Solutol HS15 as an excipient (5% Solutol HS15, 5% EtOH, 20% D_2O, 70% saline) dramatically changed the situation and made it possible for us to quantify the ^{19}F NMR signals from BLT-F_2 in those media. Furthermore, it was found that the addition of 6 equivalents of GSH (15 mM) to BLT-F_2 in this formulation showed only ca. 20% linker cleavage after 10 hours in sharp contrast to the nearly-quantitative cleavage within 1 hour in DMSO/D_2O [74]. This observation clearly indicates that excipients commonly used for *in vivo* drug efficacy studies may impose a profound effect on the stability of TTDDSs by protecting disulfide linkers from GSH-mediated cleavage.

3.3. ^{19}F NMR analysis of the plasma stability and drug release using BLT-S-F_6 as a probe

3.3.1. Effects of solvent systems and drug formulations on the ^{19}F NMR chemical shifts of the CF_3 groups at the 3′ position of SB-T-12822-5 and the taxoid moiety in BLT-S-F_6—Following up the interesting findings with BLT-F_2 described above, we investigated the utility of more sensitive "3-FABS" probe system, BLT-S-F_6, wherein the 3′-CF_3 and *m*-CF_3O groups of free taxoid (SB-T-12822-5) and probe (BLT-S-F_6) should serve as reporter ^{19}F signals to assess the stability and reactivity of the probe [74]. The differences in the ^{19}F chemical shifts of 3′-CF_3 and *m*-CF_3O groups between the probe and free taxoid were determined (370 MHz ^{19}F NMR) in various solvent and formulation systems. Results are summarized in Table 6 [74].

As Table 6 shows (Entry 1), nearly 0.3 ppm chemical shift difference with baseline resolution was observed between the 3′-CF_3 groups of the probe (−73.116 ppm) and free taxoid (−73.404 ppm). In contrast, the chemical shift difference between the 2-*m*-OCF_3 groups of the probe (−57.923 ppm) and free taxoid (−57.961 ppm) was a much smaller, as anticipated (Entry 1). Next, the ^{19}F NMR chemical shift differences between the same two pairs of reporter signals were measured in various biologically relevant media with or without excipient. Gratifyingly, substantial chemical shift difference between the 3′-CF_3 signals of the probe and free taxoid was observed on using polysorbate 80 as the excipient (Entries 2–4) with as large as 0.21 ppm difference with baseline resolution in blood plasma (Entry 2). In contrast, however, no appreciable chemical shift difference was observed when Solutol HS15 was employed as the excipient (Entry 9). The results strongly suggest that different excipients would make different microenvironments to probe BLT-S-F_6, and this finding is not only for BLT-S-F_6, but also applicable to a variety of drugs and drug conjugates. In the absence of excipient, the ^{19}F NMR chemical shift differences between the pair of 3′-CF_3 reporter signals were much smaller (i.e., 0.070–0.046 ppm) (Entries 5–8). For the 2-*m*-CF_3O signals, no chemical shift difference was observed between the pair of reporter signals in the presence of an excipient, while small differences were detected (0.02–0.04 ppm) (Entries 1, 5–8).

3.3.2. Assessment of the stability and reactivity of probe BLT-S-F_6 in human blood plasma by ^{19}F NMR—The stability of probe BLT-S-F_6 with 2% polysorbate 80 was examined in human blood plasma at 37 °C by ^{19}F NMR using the 3′-CF_3 signals of the

probe (−73.048 ppm) and released free taxoid (−72.838 ppm) [74]. As Fig. 9 shows, the probe (**P**) remained stable with a minute release of of taxoid (**T**) for 48 hours in blood plasma, which suggests that the putative half-life of this drug conjugate, as well as TTDDSs using this self-immolative linker unit in this formulation would be longer than one week in human blood plasma.

Next, we investigated the reactivity of the probe BLT-S-F_6 with GSH under the conditions mimicking the GSH concentration in tumor (10 mM level) [75], wherein the cleavage of the disulfide linker and thiolactonization should take place in a reasonable time frame. Thus, GSH (100 equiv., 20 mM concentration) was added to the probe in human blood plasma and the kinetic behavior of the probe was analyzed by time-resolved ^{19}F NMR spectroscopy at 37 °C. As Fig. 10 shows, >98% of the probe (**P**) disappeared within 10 hours with appearance of the corresponding amount of fee taxoid (**T**). The plotting the changes in integration of the C3′-CF_3 signals of the probe (**P**) and free taxoid (**T**) is shown in Fig. 11, from which the half-life of the probe (**P**) was calculated to be ca. 3 h. This experiment provided an excellent estimate for the half-life, as well as the complete conversion of this self-immolative disulfide linker in the cytosolic compartments following RME.

It was found that the linker cleavage and drug release of the probe with 100 equivalents of GSH in D_2O containing 2% polysorbate 80 and 2% EtOH at 37 °C was significantly slower than that in blood plasma under the same conditions wherein only 50% drug release was observed at approximately 4 days. Since blood plasma contains many proteins, which are not present in the D_2O or saline/PBS formulations, these proteins are likely to interact with the excipient, leading to its dissociation from the drug conjugate. Thus, in the blood plasma, the disulfide linkage would be more exposed to the attack of GSH.

4. Concluding Remarks

Novel 3′-difluorovinyltaxoids were strategically designed to block the metabolism by cytochrome P-450 3A4 enzyme, synthesized and evaluated for their cytotoxicity against drug-sensitive and drug-resistant human cancer cell lines. Molecular modeling study indicated that a difluorovinyltaxoid binds to β-tubulin in a manner that is consistent with the REDOR-Taxol structure. The difluorovinyl group appears to mimic the isobutenyl group pretty well although it is smaller in size with very different electronic property. These novel fluorotaxoids exhibited several to 16 times better activity against MCF7, HT-29 and PANC-1 cell lines and up to three orders of magnitude higher potency against NCI/ADR cell line as compared to paclitaxel. More impressively, one of the 3′-difluorovinyltaxoids, SB-T-12854, exhibited 230-33,000 times higher potency than conventional anticancer drugs against CSC-enriched HCT-116 cell line. Since CSCs have been shown to be responsible for tumor metastasis and reoccurrence, this is a quite significant finding. New-generation taxoids, including 3′-difluorovinyltaxoids, were found to suppress the expression of “stemness genes”, promoting differentiation of the treated CSCs, which appears to have revealed a new mechanism of action (MOA) for taxoid anticancer agents.

3′-Difluorovinyltaxoids induced GTP-independent tubulin polymerization much faster than paclitaxel, and the resulting microtubules were stable to Ca^{2+}-induced depolymerization, as

anticipated. Based on the morphology analysis by electron microscopy, the formation of a large number of thinner, shorter and straight microtubules, which is consistent with the very rapid tubulin polymerization mentioned above, appears to be unique to difluorovinyltaxoids.

The binding of SB-T-12854 to microtubules was shown to be ca. 10 times stronger than paclitaxel and slightly better than SB-T-1214. Also, it has been shown that the binding of SB-T-12854 is much less exothermic than that of paclitaxel with a large decrease in the enthalpy of binding, but this decrease in the enthalpy of binding is compensated by a substantial increase in the entropy of binding, which suggests significant differences in the binding mechanism.

Consequently, novel 3′-difluorovinyltaxoids would serve as powerful cytotoxic agents in tumor-targeted drug delivery systems (TTDDSs) with their very high potency, especially against CSCs, metabolic stability, and unique MOA.

Two novel ^{19}F NMR probes, BLT-F_2 and BLT-S-F_6, were designed by strategically incorporating fluorine, CF_3 and CF_3O groups into tumor-targeting drug conjugates, bearing biotin as the tumor-targeting module, a self-immolative disulfide linker unit, and fluorotaxoids as cytotoxic agents. These ^{19}F-probes were designed and synthesized to investigate the mechanism of linker cleavage and factors that influence their plasma and metabolic stability by real-time ^{19}F NMR analysis. Time-resolved ^{19}F NMR study on probe BLT-F_2 revealed a stepwise mechanism for the release of a fluorotaxoid, which might not be detected by other analytical methods.

The stability of probe BLT-F_2 was found to be dramatically enhanced on using an excipient. Thus, the effects of excipients on the stability and reactivity of drug conjugates bearing a self-immolative disulfide linker unit were further studied by using probe BLT-S-F_6. This probe was designed to have enhanced sensitivity by introducing CF_3 and CF_3O groups to the taxoid component. Indeed, probe BLT-S-F_6 has been shown to be very useful to study the stability and reactivity of the drug delivery system in human blood plasma by ^{19}F NMR. The use of polysorbate 80 as excipient for the formulation of probe BLT-S-F_6 was found to dramatically increase the stability of the disulfide linker system. Thus, the half-life of the probe in human blood plasma was estimated to be longer than one week, while the free taxoid was released smoothly ($t_{1/2}$ ~3 hours) in the presence of GSH (20 mM), which is equivalent to the level of GSH in tumors, and thus mimics the drug release in cancer cells.

Although the clean analysis of the linker stability and reactivity of drug conjugates in blood plasma or cell culture media by HPLC and ^{1}H NMR is very challenging, it is demonstrated that the use of ^{19}F NMR can provides a practical solution to this problem.

Further studies on the strategic incorporation of fluorine and organofluorine groups into new-generation taxoids and their applications to chemical biology, medicinal chemistry, drug discovery and development are actively in progress in our laboratory.

Acknowledgments

This work has been supported by grants from the National Institutes of Health (GM42798 and CA103314 to I.O.). Generous support from Indena SpA is gratefully acknowledged.

References

1. Ojima, I. Fluorine in Medicinal Chemistry and Chemical Biology. Wiley-Blackwell; Chichester: 2009.
2. Muller K, Faeh C, Diederich F. Science. 2007; 317:1881–1886. [PubMed: 17901324]
3. Begue J-P, Bonnet-Delpon D. J Fluorine Chem. 2006; 127:992–1012.
4. Isanbor C, O'Hagan D. J Fluorine Chem. 2006; 127:303–319.
5. (a) Wang J, Sánchez-Roselló M, Aceña JL, del Pozo C, Sorochinsky AE, Fustero S, Soloshonok VA, Liu H. Chem Rev. 2014; 114:2432–2506. [PubMed: 24299176] (b) Zhou Y, Wang J, Gu Z, Wang S, Zhu W, Aceña JL, Soloshonok VA, Izawa K, Liu H. Chem Rev. 2016; 116:422–518. [PubMed: 26756377]
6. Cottet F, Marull M, Lefebvre O, Schlosser M. Eur J Org Chem. 2003; 2003:1559–1568.
7. Kirk KL. J Fluorine Chem. 2006; 127:1013–1029.
8. Yamazaki, T., Taguchi, T., Ojima, I. Fluorine in Medicinal Chemistry and Chemical Biology. Ojima, I., editor. Wiley-Blackwell; Chichester: 2009. p. 3-46.
9. Jaracz S, Chen J, Kuznetsova L, Ojima I. Bioorg Med Chem. 2005; 13:5043–5054. [PubMed: 15955702]
10. Farokhzad OC, Cheng J, Teply BA, Sherifi I, Jon S, Kantoff PW, Richie JP, Langer R. Proc Nat Acad Sci. 2006; 103:6315–6320. [PubMed: 16606824]
11. Chu TC, Marks JW III, Lavery LA, Faulkner S, Rosenblum MG, Ellington AD, Matthew Levy M. Cancer Res. 2006; 66:5989–5992. [PubMed: 16778167]
12. Ducry L, Stump B. Bioconjugate Chem. 2010; 21:5–13.
13. Xia W, Low P. J Med Chem. 2010; 53:6811–6824. [PubMed: 20666486]
14. Ojima I, Zuniga E, Berger W, Seitz J. Future Med Chem. 2012; 4:33–50. [PubMed: 22168163]
15. Ojima I. ChemBioChem. 2004; 5:628–635. [PubMed: 15122634]
16. Ojima I. Acc Chem Res. 2008; 41:108–119. [PubMed: 17663526]
17. Chen S, Zhao X, Chen J, Chen J, Kuznetsova L, Wong S, Ojima I. Bioconjugate Chem. 2010; 21:979–987.
18. Dalerba P, Cho RW, Clarke MF. Annu Rev Med. 2007; 58:267–284. [PubMed: 17002552]
19. Botchkina GI, Zuniga ES, Das M, Wang Y, Wang H, Zhu S, Savitt AG, Rowehl R, Leyfman Y, Ju J, Shroyer K, Ojima I. Mol Cancer. 2010; 9:192–204. [PubMed: 20630067]
20. Botchkina GI, Zuniga ES, Park R, Rowehl RH, Bhalla R, Bialkowska AB, Zhang Y, Johnson F, Golub LM, Ojima I, Shroyer KR. PLoS ONE. 2013; 8:e69884:69881–69815. [PubMed: 24086245]
21. Rowinsky E. Annu Rev Med. 1997; 48:353–374. [PubMed: 9046968]
22. Bono JD, Oudard S, Ozguroglu M, Hansen S, Machiels J, Shen L, Matthews P, Sartor A. J Clin Oncol. 2010; 28:s4508.
23. Ojima I, Lichtenthal B, Lee S, Wang C, Wang X. Expert Opin Ther Patents. 2016; 26:1–20.
24. Ojima, I., Kamath, A., Seitz, JD. Natural Products in Medicinal Chemistry. Hanessian, S., editor. Wiley-VCH; Weinheim: 2013. p. 127-180.
25. Bissery M, Nohynek G, Sanderink G, Lavelle F. Anticancer Drugs. 1995; 6:339–355. [PubMed: 7670132]
26. Fojo A, Ueda K, Slamon D, Poplack D, Gottesman M, Pastan I. Proc Nat Acad Sci. 1987; 84:265–269. [PubMed: 2432605]
27. Gottesman M, Pastan I. Annu Rev Biochem. 1993; 62:385–427. [PubMed: 8102521]
28. Ojima I, Das M. J Nat Prod. 2009; 72:554–565. [PubMed: 19239240]
29. Pepe, A., Kuznetsova, L., Sun, L., Ojima, I. Fluorine in Medicinal Chemistry and Chemical Biology. Ojima, I., editor. Wiley-Blackwell; Chichester: 2009. p. 117-139.
30. Ojima I, Chen J, Sun L, Borella C, Wang T, Miller M, Lin S, Geng X, Kuznetsova L, Qu C, Gallagher G, Zhao X, Zanardi I, Xia S, Horwitz S, Clair JS, Guerriero J, Bar-Sagi D, Veith J, Pera P, Bernacki R. J Med Chem. 2008; 51:3203–3221. [PubMed: 18465846]

31. Kuznetsova L, Pepe A, Ungureanu I, Pera P, Bernacki R, Ojima I. J Fluorine Chem. 2008; 129:817–828.
32. Kuznetsova L, Sun L, Chen J, Zhao X, Seitz J, Das M, Li Y, Veith J, Pera P, Bernacki R, Xia S, Horwitz S, Ojima I. J Fluorine Chem. 2012; 143:177–188.
33. Ojima, I., Kuduk, SD., Slater, JC., Gimi, RH., Sun, CM., Chakravarty, S., Ourevitch, M., Abouabdellah, A., Bonnet-Delpon, D., Begue, J-P., Veith, JM., Pera, P., Bernacki Ralph, J. Biomedical Frontiers of Fluorine Chemistry. Ojima, I.McCarthy, JR., Welch, JT., editors. American Chemical Society; Washington, D. C: 1996. p. 228-243.ACS Symposium Series 639
34. Seitz J, Vineberg JG, Zuniga ES, Ojima I. J Fluorine Chem. 2013; 152:157–165.
35. Cobb S, Murphy C. J Fluorine Chem. 2009; 130:132–143.
36. Ojima I, Slater J, Michaud E, Kuduk S, Bounaud P-Y, Vrignaud P, Bissery M, Veith J, Pera P, Bernacki R. J Med Chem. 1996; 39:3889–3896. [PubMed: 8831755]
37. Ojima I, Wang T, Miller ML, Lin S, Borella CP, Geng X, Pera P, Bernacki RJ. Bioorg Med Chem Lett. 1999; 9:3423–3428. [PubMed: 10617084]
38. Ojima I, Lin S, Slater JC, Wang T, Pera P, Bernacki RJ, Ferlini C, Scambia G. Bioorg Med Chem. 2000; 8:1619–1628. [PubMed: 10976509]
39. Kuznetsova L, Ungureanu IM, Pepe A, Zanardi I, Wu X, Ojima I. J Fluorine Chem. 2004; 125:487–500.
40. Gut I, Ojima I, Vaclavikova R, Simek P, Horsky S, Linhart I, Soucek P, Knodrova E, Kuzetsova L, Chen J. enobiotica. 2006; 36:772–792.
41. Geney R, Sun L, Pera P, Bernacki Ralph J, Xia S, Horwitz Susan B, Simmerling Carlos L, Ojima I. Chem Biol. 2005; 12:339–348. [PubMed: 15797218]
42. Sun L, Simmerling C, Ojima I. ChemMedChem. 2009; 4:719–731. [PubMed: 19360801]
43. Voborilova J, Nemcoa-Furstova V, Neubauerova J, Ojima I, Zanardi I, Gut I, Kovar J. Invest New Drugs. 2011; 29:411–423. [PubMed: 20013348]
44. Zuniga, ES. PhD Dissertation. Stony Brook University; 2012.
45. Li F, Tiede B, Massague J, Kang Y. Cell Res. 2007; 17:3–14. [PubMed: 17179981]
46. Jelínek M, Balušíková K, Fidlerová J, Němcová-Fürstová V, Kopperová D, Šrámek J, Zanardi I, Ojima I, Kovář J. Cancer Cell Int. 2013; 13:42. [PubMed: 23672670]
47. Matesanz R, Trigili C, Rodríguez-Salarichs J, Zanardi I, Pera B, Nogales A, Fang W-S, Jímenez-Barbero J, Canales Á, Barasoain I, Ojima I, Díaz JF. Bioorg Med Chem. 2014; 22:5078–5090. [PubMed: 25047938]
48. Ojima I, Kumar K, Awasthi D, Vineberg JG. Bioorg Med Chem. 2014; 22:5060–5077. [PubMed: 24680057]
49. Ehrlichová M, Ojima I, Václavíková R, Němcová-Fürstová V, Vobořilová J, Šimek P, Horský S, Souček P, Kovár J, Gut I. N-S Arch Pharmacol. 2012; 385:1035–1048.
50. Marre F, Sanderink F-J, Sousa Gd, Gaillard C, Martinet M, Rahmani R. Hepatic Cancer Res. 1996; 56:1296–1302. [PubMed: 8640817]
51. Monsarrat B, Mariel E, Cros S, Gares M, Guenard D, Gueritte-Voegelein F, Wright M. Drug Metab Dispos. 1990; 18:895–901. [PubMed: 1981534]
52. Cresteil T, Monsarrat B, Alvinerie P, Treluyer J, Vleira I, Wright M. Cancer Res. 1994; 54:386–392. [PubMed: 7903909]
53. Chari RVJ, Miller ML, Widdison WC. Angew Chem Int Ed. 2014; 53:3796–3827.
54. Chen J, Jaracz S, Zhao X, Chen S, Ojima I. Exp Opin Drug Deliv. 2005; 2:873–890.
55. Ojima I, Geng X, Wu X, Qu C, Borella CP, Xie H, Wilhelm SD, Leece BA, Bartle LM, Goldmacher VS, Chari RV. Med Chem. 2002; 45:5620–5623.
56. Zolot RS, Basu S, Million RP. Nature Rev Drug Discov. 2013; 12:259–260. [PubMed: 23535930]
57. Carter PJ, Senter PD. Cancer J. 2008; 14:154–169. [PubMed: 18536555]
58. Leamon CP. Curr Opin Invest Drugs. 2008; 9:1277–1286.
59. Vlahov I, Santhapuram H, Kleindl P, Howard S, Stanford K, Leamon C. Bioorg Med Chem Lett. 2006; 16:5093–5096. [PubMed: 16870437]

60. Vineberg JG, Zuniga ES, Kamath A, Chen Y-J, Seitz JD, Ojima I. J Med Chem. 2014; 57:5777–5791. [PubMed: 24901491]
61. Chen J, Chen S, Zhao X, Kuznetsova L, Wong S, Ojima I. J Am Chem Soc. 2008; 130:16778–16785. [PubMed: 19554734]
62. Seitz JD, Vineberg JG, Herlihy E, Park B, Melief E, Ojima I. Bioorg Med Chem. 2015; 23:2187–2194. [PubMed: 25819334]
63. Vineberg JG, Wang T, Zuniga ES, Ojima I. J Med Chem. 2015; 58:2406–2416. [PubMed: 25654690]
64. Gerig JT. Methods Enzymol. 1989; 177:3–23. [PubMed: 2607985]
65. Dalvit C, Ardini E, Flocco M, Fogliatto GP, Mongelli N, Veronesi M. J Am Chem Soc. 2003; 125:14620–14625. [PubMed: 14624613]
66. Dalvit C. Prog Nucl Magn Res Spect. 2007; 51:243–271.
67. Keita M, Kaffy J, Troufflard C, Morvan E, Crousse B, Ongeri S. Org Biomol Chem. 2014; 12:4576–4581. [PubMed: 24867821]
68. Ojima I, Kuduk SD, Chakravarty S, Ourevitch M, Bégué J-P. J Am Chem Soc. 1997; 119:5519–5527.
69. Ojima, I., Inoue, T., Slater, JC., Lin, S., Kuduk, SC., Chakravarty, S., Walsh, JJ., Gilchrist, L., McDermott, AE., Cresteil, T., Monsarrat, B., Pera, P., Bernacki, RJ. Asymmetric Fluoroorganic Chemistry: Synthesis, Application, and Future Directions. Ramachandran, PV., editor. American Chemical Society; Washington, D. C: 1999. p. 158-181.ACS Symp. Ser. 746
70. Ojima I, Inoue T, Chakravarty S. J Fluorine Chem. 1999; 97:3–10.
71. Ojima I. J Org Chem. 2013; 78:6358–6383. [PubMed: 23614876]
72. Kigawa J, Minagawa Y, Kanamori Y, Itamochi H, Cheng X, Okada M, Oisho T, Terakawa N. Cancer. 1998; 82:697–702. [PubMed: 9477102]
73. Zheng ZB, Zhu G, Tak H, Joseph E, Eiseman JL, Creighton DJ. Bioconjug Chem. 2005; 16:598–607. [PubMed: 15898727]
74. Seitz JD, Vineberg JG, Wei L, Khan JF, Lichtenthal B, Lin C-F, Ojima I. J Fluorine Chem. 2015; 171:148–161.
75. Appenzeller-Herzog C. J Cell Sci. 2011; 124:847–855. [PubMed: 21378306]

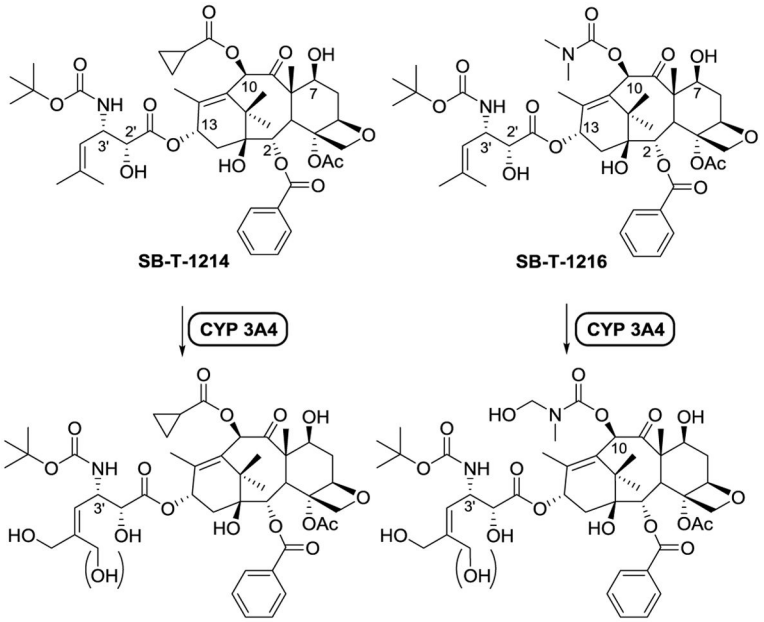

Fig. 1.

Primary sites of hydroxylation on the new-generation taxoids by the P450 family of enzymes. Adapted from Reference [32].

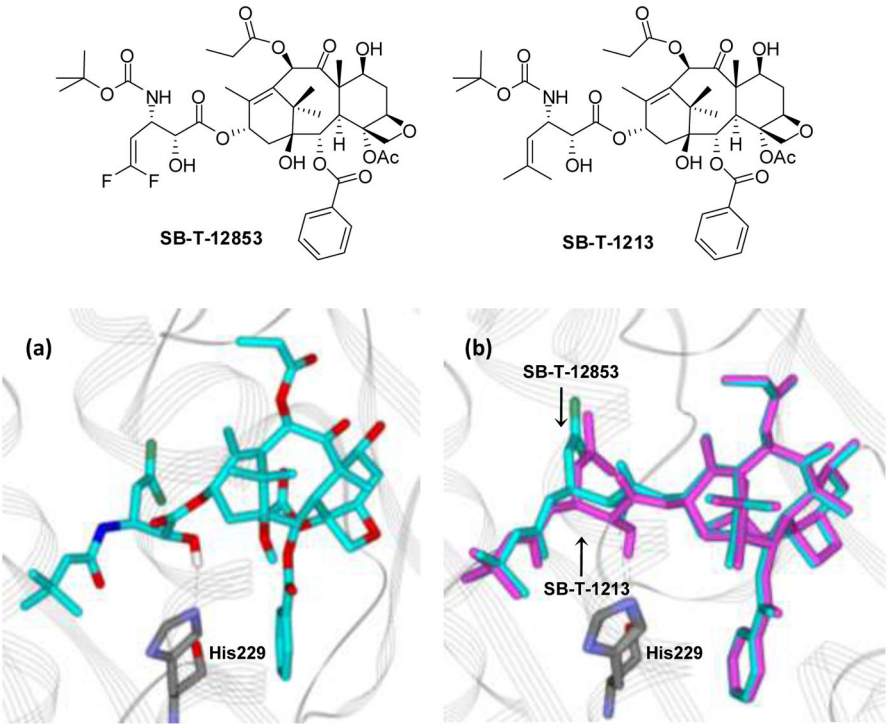

Fig. 2.

(a) Proposed binding conformation of SB-T-12853 in tubulin; (b) overlay of SB-T-12853 (cyan) and SB-T-1213 (magenta) in tubulin. Adapted from Reference [32].

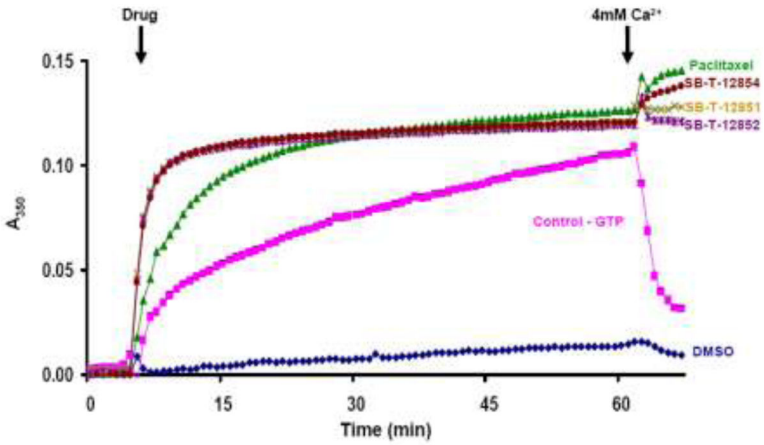

Fig. 3.

Tubulin polymerization with SB-T-12851, SB-T-12852, SB-T-12854, paclitaxel and GTP: microtubule protein 1 mg/mL, 37 °C, GTP 1 mM, Drug 10 μM. Adapted from Reference [32].

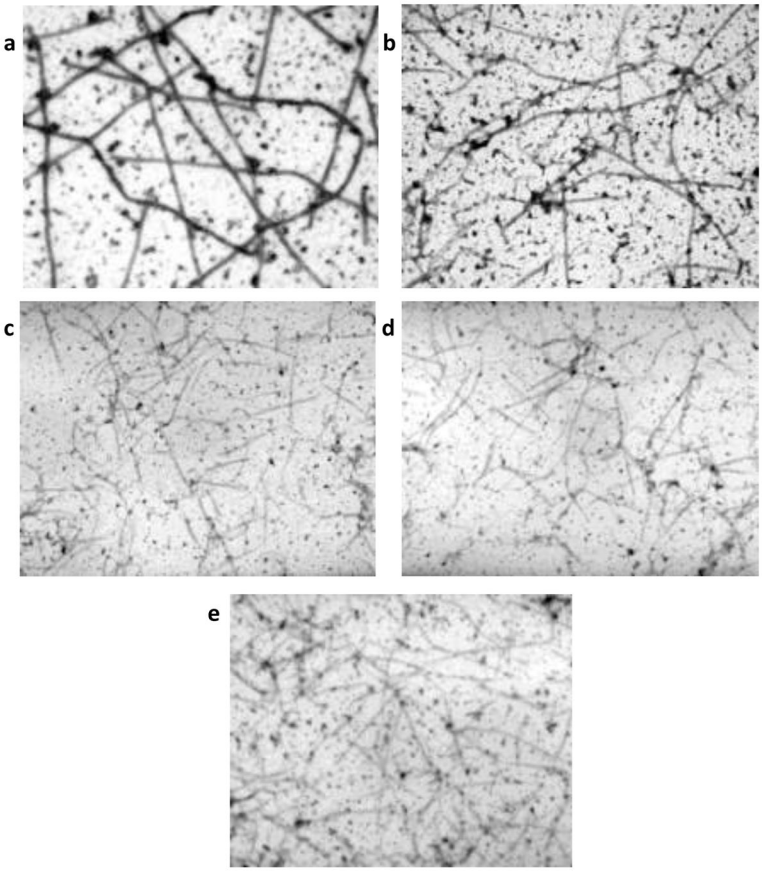

Fig. 4.

Electromicrographs of microtubules: (a) GTP; (b) paclitaxel; (c) SB-T-12851; (d) SB-T-12852; (e) SB-T-12854. Adapted from Reference [32].

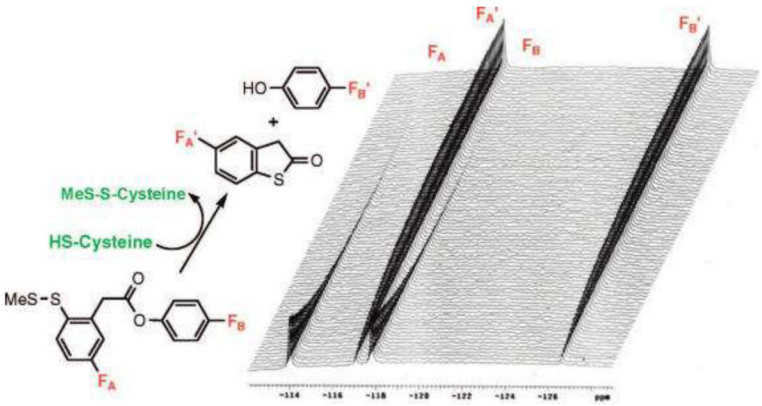

Fig. 5.

A model system for the mechanism-based drug release using cysteine as the trigger for thiolactonization. Adapted from Reference [15].

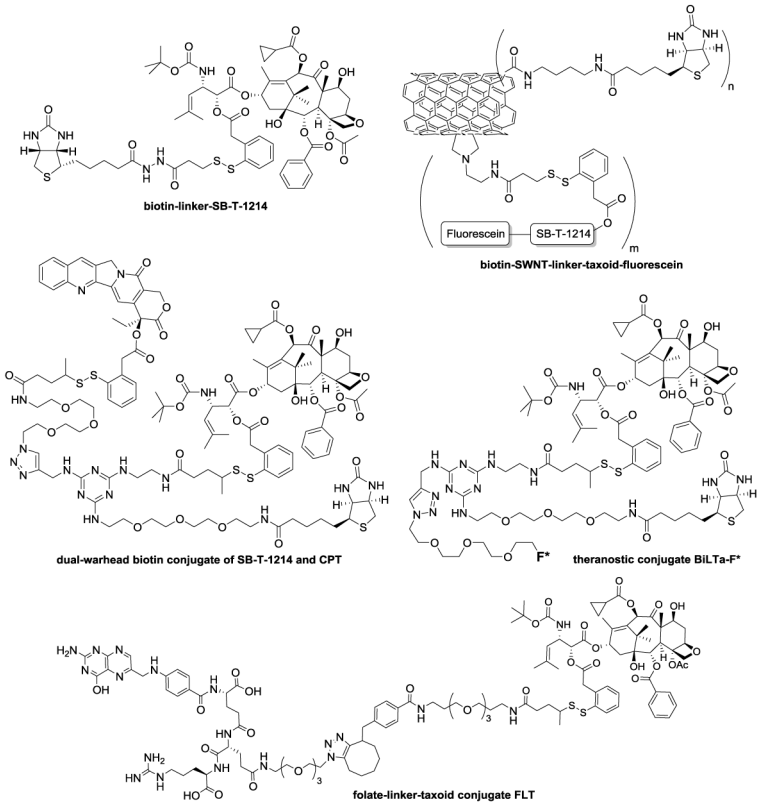

Fig. 6.
Examples of vitamin-based SMDCs developed in our laboratory.

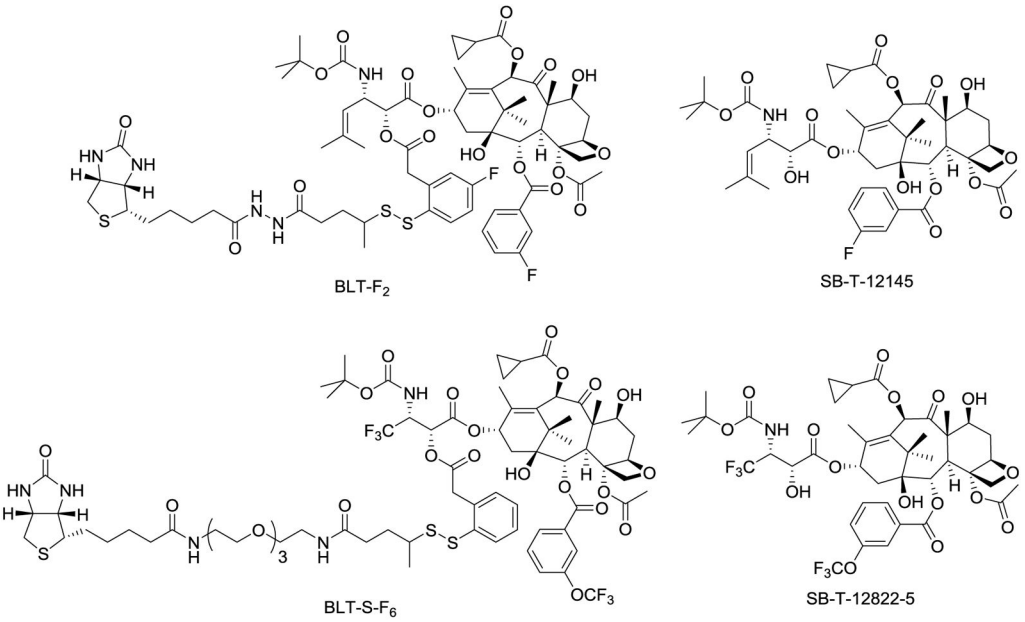

Fig. 7.
BLT-F_2, BLT-S-F_6, SB-T-12145 and SB-T-12822-5.

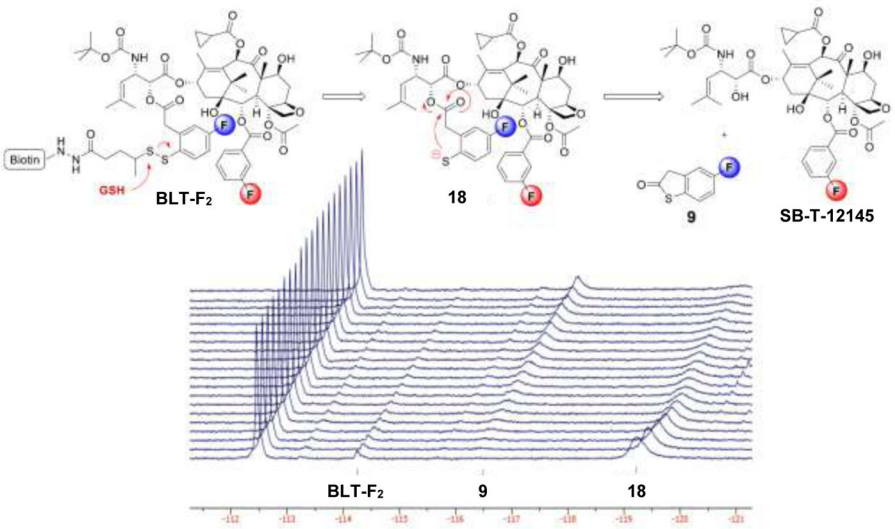

Fig. 8.

Time-resolved ^{19}F NMR spectra for the disulfide linker cleavage and thiolactonization process of BLT-F_2 (2.5 mM) in 30% DMSO in D_2O beginning at 1 hour after the addition of 6 equivalents of GSH at 25 °C with 15 min intervals (128 scans/spectrum). Adapted from Reference [74].

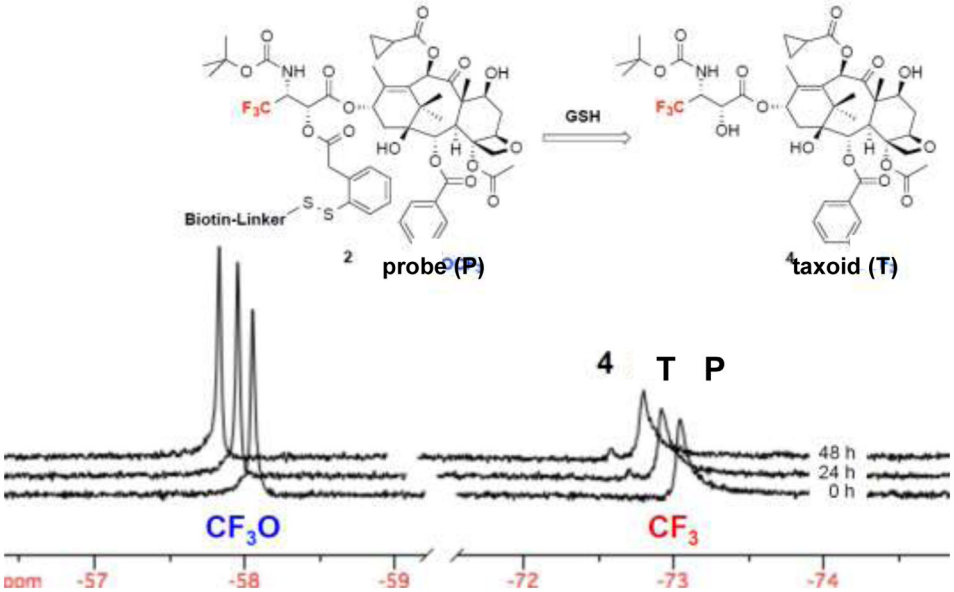

Fig. 9.

Time-resolved ^{19}F NMR spectra for the drug release of the probe (BLT-S-F_6) (200 μM) in 86% blood plasma, 10% D_2O, 2% ethanol, and 2% polysorbate 80 at 37 °C without supplemental GSH at 0, 24, and 48 h (2048 scans/spectrum). The signals of 2-*m*-OCF_3 (*left*) and 3′-CF_3 (*right*) for the probe (**P**) and free taxoid (**T**, SB-T-12822-5) are shown, which indicates minimal drug release after 48 h. Adapted from Reference [74].

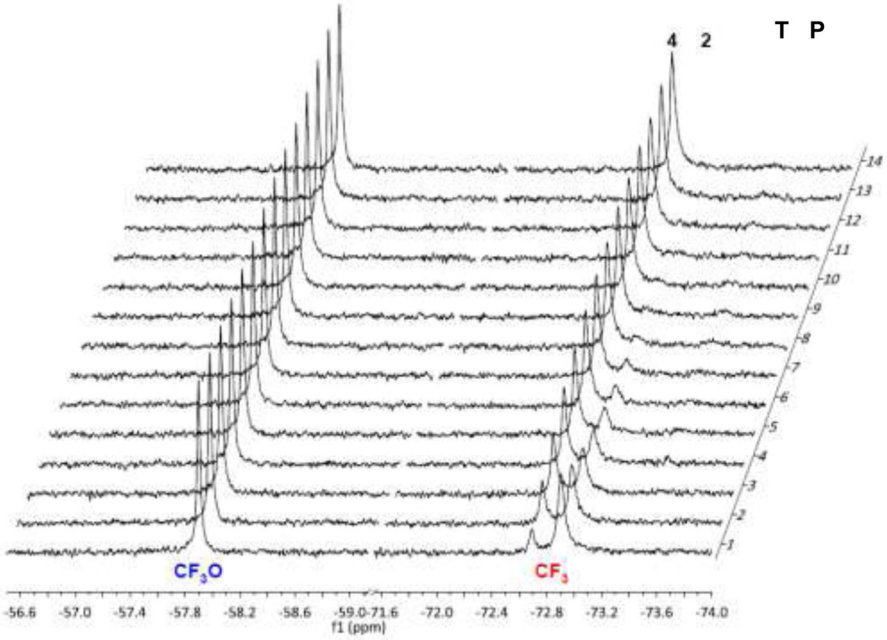

Fig. 10.

Time-resolved ^{19}F NMR spectra for the drug release of the probe (**P**, BLT-S-F_6) (200 μM) in 86% blood plasma, 2% ethanol, and 2% Tween 80 in D_2O at 30 min after the addition of 100 equivalents of GSH at 37 °C with 1 h intervals (1024 scans/spectrum) for 13 h. The signals of 2-*m*-OCF_3 (*left*) and the 3′-CF_3 (*right*) are shown, which indicate full drug (**T**, SB-T-12822-5) release after 13.5 h. Adapted from Reference [74].

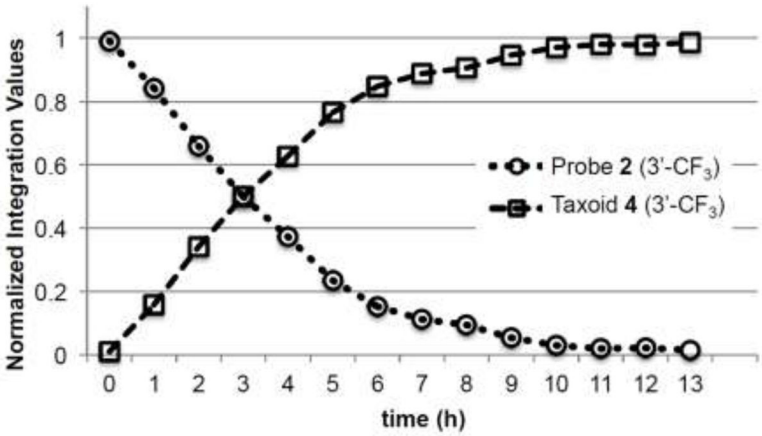

Fig. 11.

Normalized changes in integration of 3′-CF_3 peaks of the probe (BLT-S-F_6) with 100 equiv. of GSH in 86% blood plasma, 2% ethanol, 2% polysorbate 80, 10% D_2O and released free taxoid (SB-T-12822-5). Adapted from Reference [74].

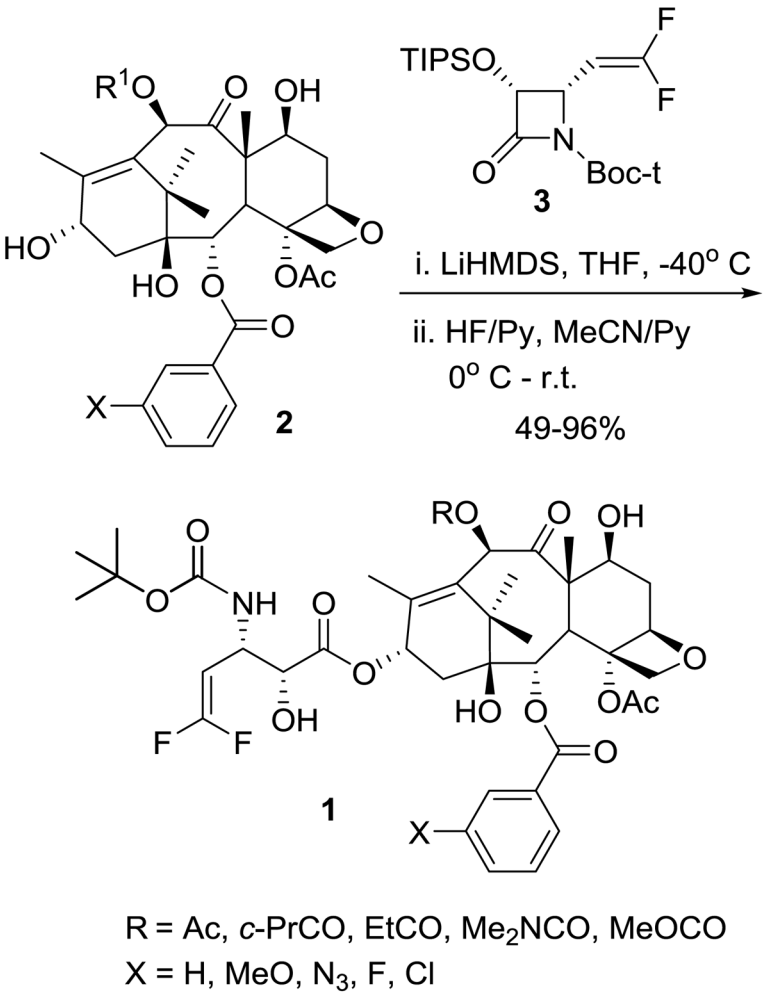

Scheme 1.

Synthesis of 3′-difluorovinyltaxoids **1** through the Ojima-Holton coupling.

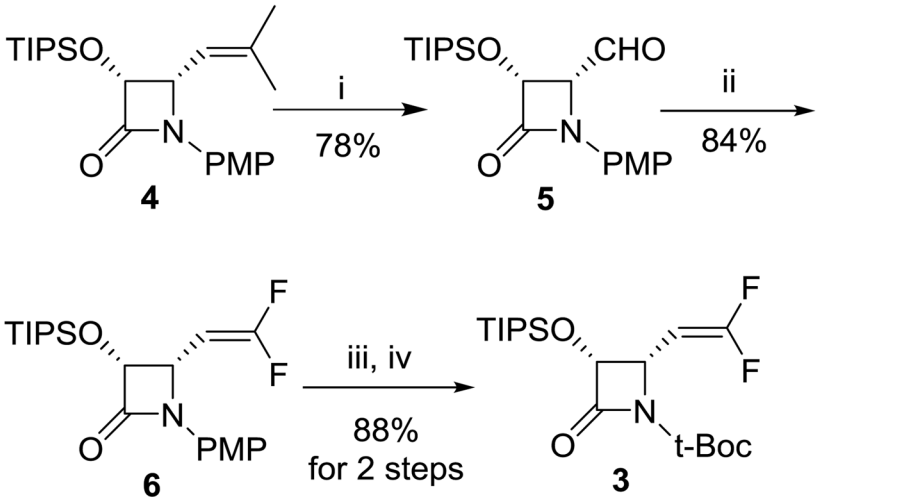

i) O_3, MeOH/CH_2Cl_2, -78 °C, Me_2S; ii) HMPT, CF_2Br_2, Zn, THF, 0 °C -> reflux; iii) CAN, MeCN/H_2O, -10 °C; iv) Boc_2O, Et_3N, DMAP, CH_2Cl_2, r.t.

Scheme 2.

Preparation of (3*R*,4*R*)-1-*t*-Boc-3-TIPSO-4-difluorovinylazetidin-2-one (**3**).

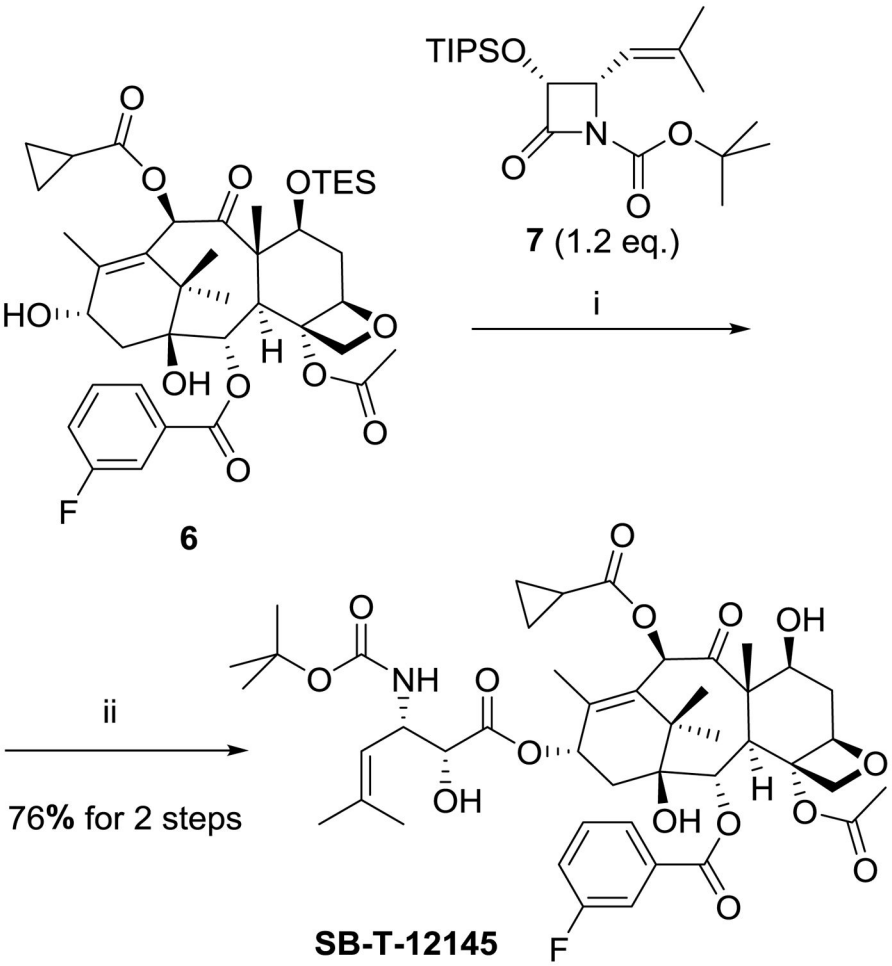

i) LHMS (1.5 eq.), THF, -40 °C, 1.5 h; ii) HF/Py, MeCN/Py, 0 °C - rt, 12 h

Scheme 3.
Synthesis of SB-T-12145.

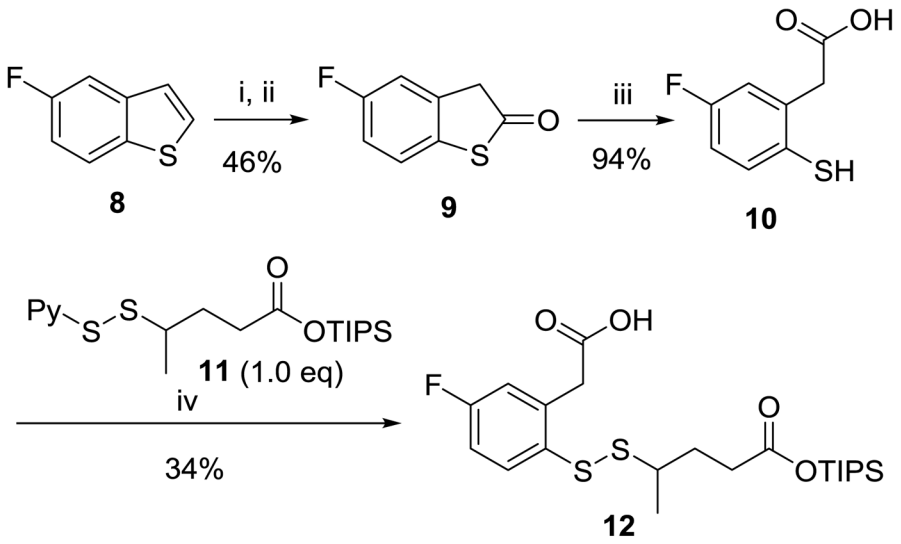

i) *n*-BuLi (1.1 eq), $B(OBu)_3$ (1.2 eq), Et_2O, -40 °C - 0 °C, 1h; ii) 30% H_2O_2, EtOH, rt, 12 h; iii) $LiOH{\cdot}H_2O$; THF/H_2O; reflux, 6 h; EtOH, 0 °C, 30 min; iv) EtOH, 0 °C, 30 min

Scheme 4.
Synthesis of ^{19}F-labeled linker construct **12**.

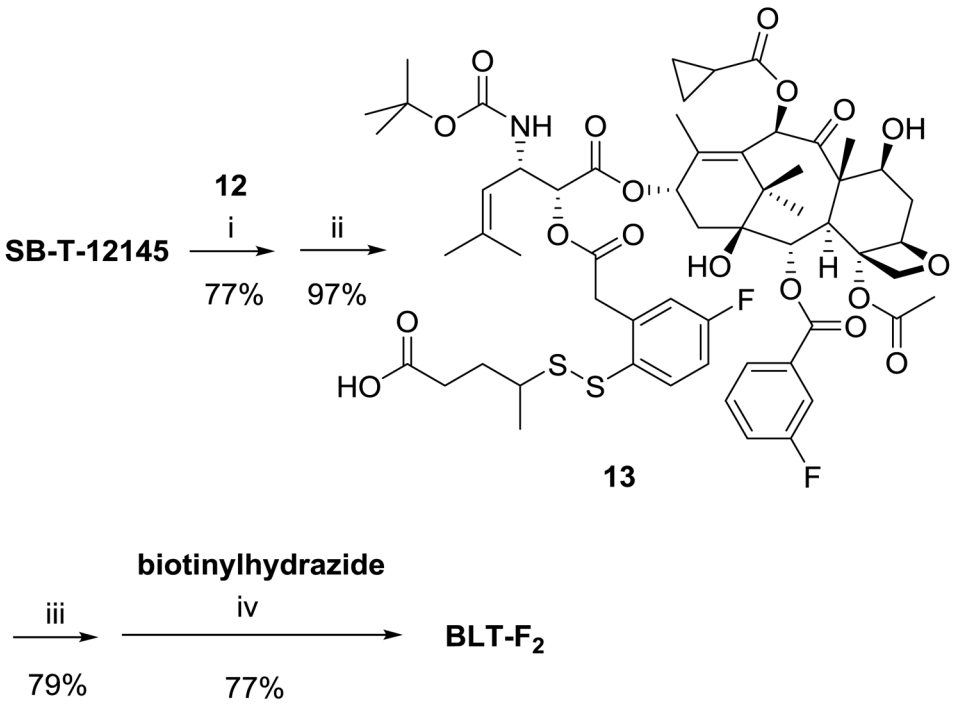

i) **12** (1.2 eq.), DIC (1.3 eq), DMAP (0.3 eq), CH_2Cl_2, -10 °C - rt, 4 h; ii) HF/Py, CH_3CN/Py, 0 °C - rt, 12 h; iii) HOSu (1.3 eq), DIC (1.1 eq), DMAP (0.3 eq), CH_2Cl_2, 0 °C - rt, 6 h; iv) **biotinylhydrazide** (1.5 eq.), DMSO/Py, rt, 3 d.

Scheme 5.
Synthesis of BLT-F_2.

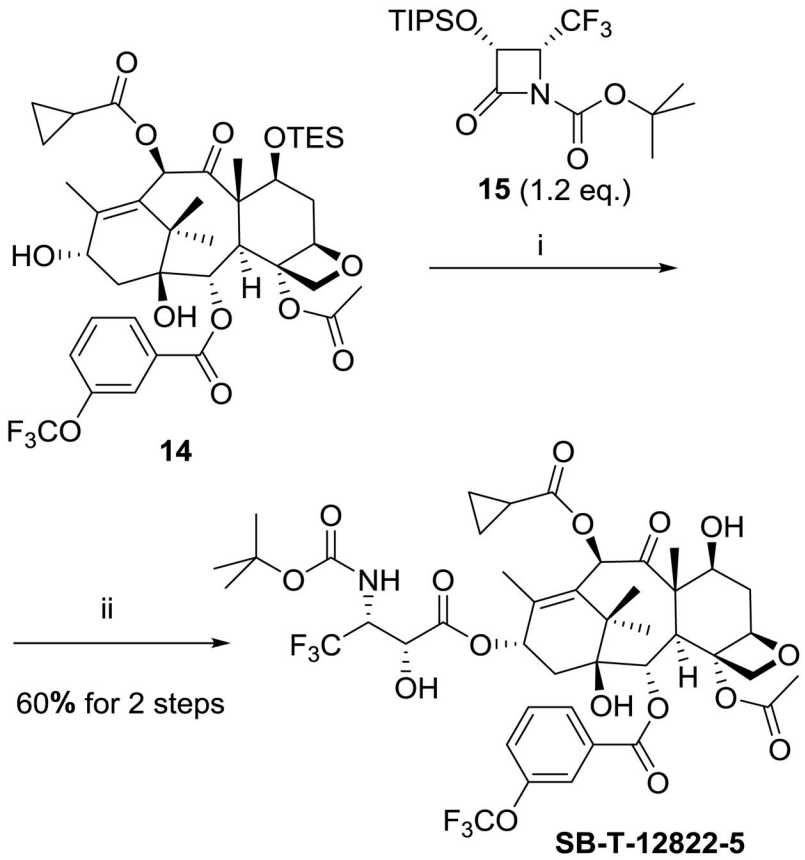

i) LHMS (1.5 eq.), THF, -40 °C, 3 h; ii) HF/Py, MeCN/Py, 0 °C - rt, 12 h

Scheme 6.

Synthesis of SB-T-12822-5.

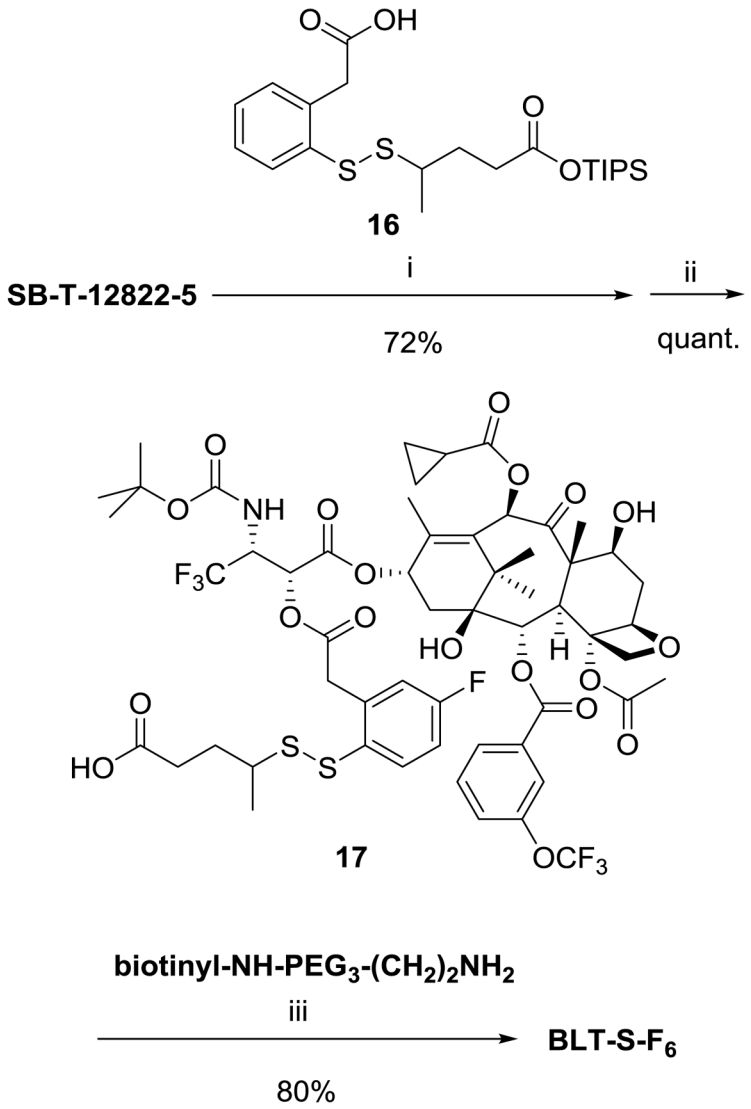

i) **16** (1.1 eq.), DIC (1.3 eq), DMAP (0.3 eq), CH_2Cl_2, rt, 24 h; ii) HF/Py, CH_3CN/Py, 0 °C - rt, 10 h; iii) **biotinyl-NH-PEG$_3$-(CH$_2$)$_2$NH$_2$** (1.1 eq.), EDC.HCl (1.2 eq.), DMAP (1.0 eq.), CH_2Cl_2, rt, 12h.

Scheme 7.
Synthesis of BLT-S-F_6

Table 1

In vitro cytotoxicity (IC_{50} nM)[a] of selected 3′-difluorovinyltaxoids

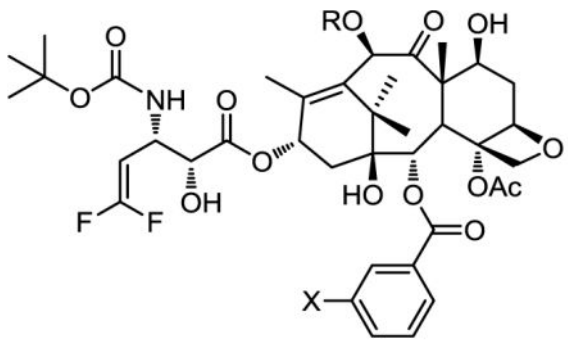

entry	taxoid	R	X	MCF7-S[b] (breast)	NCI/ADR[c] (ovarian)	R/S[d]	HT-29[e] (colon)	PANC-1[f] (pancreatic)
1	paclitaxel			1.2	300	250	3.6	25.7
2	SB-T-12851	Ac	H	0.099	0.95	9.6	0.41	1.19
3	SB-T-12852	c-Pr-CO	H	0.12	6.0	50	0.85	5.85
4	SB-T-12853	Et-CO	H	0.12	1.2	10	0.34	0.65
5	SB-T-12854	Me_2N-CO	H	0.13	4.3	33	0.46	1.58
6	SB-T-12852-1	c-Pr-CO	MeO	0.092	0.48	5.2	…	…
7	SB-T-12855-1	MeO-CO	MeO	0.078	0.50	6.4	…	…
8	SB-T-12852-2	c-PrCO	F	0.071	1.72	24	…	…
9	SB-T-12851-3	Ac	N_3	0.092	0.34	3.7	…	…
10	SB-T-12852-3	c-Pr-CO	N_3	0.092	0.45	4.9	…	…
11	SB-T-12855-3	MeO-CO	N_3	0.078	0.40	5.3	…	…
12	SB-T-12855-4	MeO-CO	Cl	0.099	1.16	12	…	…

[a]The concentration of compound inhibits 50% of the growth of a cancer cell line after 72 h drug exposure;

[b]human breast carcinona;

[c]multidrug-resistant human ovarian carcinoma;

[d]Resistance factor = (IC_{50} for drug resistant cell line, R)/ (IC_{50} for drug-sensitive cell line, S).

[e]Human colon cancer cell line.

[f]human pancreatic cancer cell line.

Table 2

Cytotoxicity (IC_{50} nM) of standard anticancer drugs and new-generation taxoids against CSC-enriched (CD133++) HCT-116 human colon cancer cell line

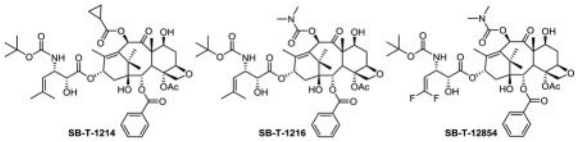

Anticancer agent	IC50 (nM)
cisplatin	4,540±276
doxorubicin	78.0±28.2
methotrexate	32.7±11.2
paclitaxel	33.8±3.33
topotecan	451±12
SB-T-1214	0.28±0.10
SB-T-1216	0.83±0.05
SB-T-12854	**0.14±0.05**

Author Manuscript

Author Manuscript

Author Manuscript

Table 3

Critical concentration (μM) of tubulin required for microtubule assembly

Compound	tubulin concentration
DMSO (vehicle)	> 200
Paclitaxel	4.2±0.2
SB-T-1214	0.9±0.2
SB-T-12854	**0.3±0.1**

Table 4

Binding constants of taxanes with microtubules ($x10^7$ M^{-1})

Compound	**26 °C**	**37 °C**
Paclitaxel	2.64±0.17	1.07±0.11
SB-T-1214	12±2	7±1
SB-T-12854	**15±3**	**10±1**

Table 5

Thermodynamic parameters of binding of taxanes to microtubules

Compound	ΔG 35°C (kJ/mol)	ΔH (kJ/mol)	ΔS (kJ/mol)
Paclitaxel[a]	−42.1±0.3	−51±4	−29±13
SB-T-1214	−46.6±0.6	−32±2	47±6
SB-T-12854	**−47.1±0.7**	**−28±3**	**64±10**

Table 6

^{19}F NMR chemical shifts (ppm) of probe BLT-F_6 in various formulations[a]

Entry	Formulation	Ratio	*m*-OCF_3 taxoid[b]	*m*-OCF_3 probe[c]	|Δ *m*-OCF_3|	CF_3 taxoid[b]	CF_3 probe[c]	|Δ CF_3|
1	$CDCl_3$	100	−57.961	−57.923	0.038	−73.404	−73.116	0.288
2	blood plasma:D_2O: EtOH:polysorbate 80	84:10:4:2	−58.074	−58.074	0	−72.838	−73.048	0.210
3	RPMI-1640:D_2O: EtOH:polysorbate 80	84:10:4:2	−57.906	−57.906	0	−72.705	−72.911	0.206
4	D_2O:EtOH:polysorbate 80	94:4:2	−57.888	−57.888	0	−72.702	−72.889	0.187
5	saline:EtOH:D_2O	50:40:10	−58.419	−58.436	0.017	−73.342	−73.412	0.070
6	PBS:EtOH:D_2O	50:40:10	−58.413	−58.431	0.018	−73.339	−73.404	0.065
7	DMSO:D_2O	70:30	−56.459	−56.431	0.028	−71.115	−71.068	0.047
8	D_2O:EtOH	60:40	−58.417	−58.436	0.019	−73.361	−73.407	0.046
9	D_2O:Solutol HS15:EtOH	84:8:8	−58.047	−58.047	0	−72.910	−72.910	0

[a]^{19}F NMR spectra were obtained for 200 μM solutions of taxoid[b], probe[c], and a 1:1 mixture of taxoid[b] and probe[c] in various formulations with or without excipients with 10% D_2O as the NMR solvent (>256 scans). The difference in the chemical shifts between each respective 2-*m*-OCF_3 and 3′-CF_3 was calculated.

[b]taxoid = SB-T-12822-5

[c]probe = BLT-S-F_6

Adapted from Reference [74]